Analyst

Integrated on-site collection and detection of airborne microparticle for a smartphone-based microclimate quality control

Journal:	*Analyst*
Manuscript ID	AN-ART-06-2020-001147.R1
Article Type:	Paper
Date Submitted by the Author:	21-Aug-2020
Complete List of Authors:	Ryu, Byunghoon; University of Michigan, Mechanical Engineering Chen, Jay; Ford Motor Company Kurabayashi, Katsuo ; University of Michigan, Mechanical Engineering Liang, X; University of Michigan, Mechanical Engineering Park, Younggeun; University of Michigan, Mechanical Engineering

Analyst

Integrated on-site collection and detection of airborne microparticle for a smartphone based microclimate quality control

Received 00th January 20xx,
Accepted 00th January 20xx

DOI: 10.1039/x0xx00000x

Byunghoon Ryu[a], Jay Chen[b], Katsuo Kurabayashi[a,c,d]*, Xiaogan Liang[a,c]*, and Younggeun Park[a,c]*

The rapid emergence of air-mediated diseases in micro-climates demands on-site monitoring of airborne microparticles. Such detection of airborne microparticles becomes more necessitating as the particles are highly localized and dynamically change over time. However, most existing monitoring systems rely on time-consuming sample collection and centralized off-site analysis. Here, we report a smartphone based integrated microsystem for on-site collection and detection that enables real-time detection of indoor airborne microparticles with high sensitivity. The collection device, inspired the Venturi effect, was designed to collect airborne microparticles without requiring an addition power supply. Our systematic analysis showed that the collection device was able to collect microparticles with consistent negative pressure, regardless of the particle concentration in the air sample. By incorporating a microfluidic-biochip based on inertial force to trap particles and an optoelectronic photodetector into a miniaturized device with a smartphone, we demonstrate real-time and sensitive detection of the collected airborne microparticles, such as Escherichia coli, Bacillus subtilis, Micrococcus luteus, and Staphylococcus with a particle-density dynamic range of 10^3–10^8 CFU/mL. Because of its capabilities of minimal-power sample collection, high sensitivity, and rapid detection of airborne microparticles, this integrated platform can be readily adopted by the government and industrial sectors to monitor indoor air contamination and improve human healthcare.

Introduction

Exposure of airborne microparticles poses a serious health concern in our society [1-3], causing a variety of infections [4, 5], severe respiratory diseases [6, 7], a problem in breathing[8], and allergies [9, 10]. Conventional airborne microparticle monitoring has been conducted for a remotely collected air sample in an off-site centralized laboratory. In this approach, sample analysis is usually performed with aqueous samples [11-14]. As such, the first step of airborne microparticle analysis requires the collection and transfer of microparticle from air to water by natural sediment or machine sampling. The machine sampling method involves large-scale machine-oriented sedimentation, percussion, centrifugal impingement, filtering, electrostatic attachment, and cyclonic separation [15] followed by analysis using dynamic image analysis, static laser light scattering, laser diffraction, dynamic light scattering, and sieve analysis [16-18]. Despite the technological advances in the analysis, fast sampling and accurate on-site detection of airborne microparticles is still a difficult technical task, especially in microclimates. So far, almost no analysis technique can ensure that the collected microparticle specimen reflects the original state and can be directly used in sample analysis [12, 15, 19, 20].

Recently, microfluidic-device-based detection methods to reduce time, sample volume, and labor requirements typical of the traditional approach[21-25]. Even though these microfluidic devices manifest sample-sparing and high-sensitivity detection capabilities, their operations still require a liquid-phase sample, large-scale equipment, or many auxiliary parts to provide the functions of sample collection, reagent treatment steps, and data processing (Table S1). Owing to these requirements, the implementation of the current existing approaches is prohibited for direct collection and detection of airborne parties in a gas phase. Indeed, an airborne microparticle monitoring system with high sensitivity, fast speed, and simple operating capabilities is imperative for a micro-climate setting.

[a] Department of Mechanical Engineering, University of Michigan, Ann Arbor, MI 48109. E-mail: bhryu@umich.edu, katsuo@umich.edu, xiaoganl@umich.edu, ygpark@umich.edu
[b] Ford Motor Company, Dearborn MI, USA E-mail: jchen288@ford.com
[c] Center for Integrative Research in Critical Care, University of Michigan, Ann Arbor MI, USA. E-mail: katsuo@umich.edu, xiaoganl@umich.edu, ygpark@umich.edu
[d] Department of Electrical Engineering and Computer Science, University of Michigan, Ann Arbor MI, USA. E-mail: katsuo@umich.edu
†Electronic Supplementary Information (ESI) available: See DOI: 10.1039/x0xx00000x
*Corresponding authors

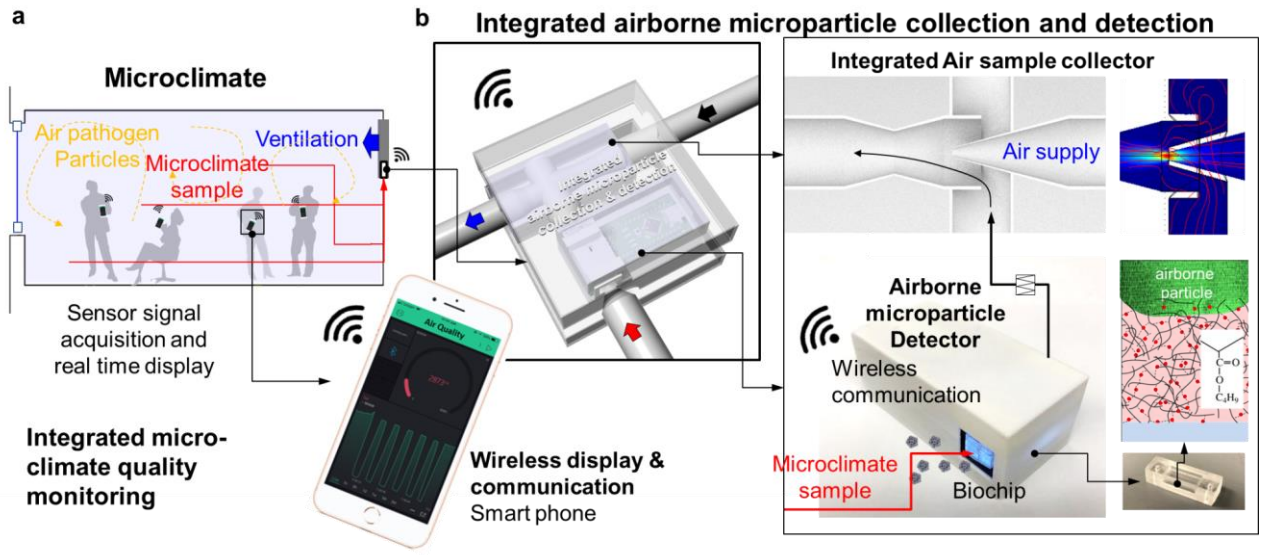

Fig. 1 Integrated airborne microparticle sample collection and detection for micro-climate quality monitoring. a) Microclimate climate quality monitoring using the integrated airborne microparticle collection and detection. The quality is monitored using a smartphone-based wireless display and communication. b) The schematic diagram shows an integrated system of air sample collection and a miniaturized detection to access the level of the airborne microparticle inside a shared microclimate space. The entire platform is integrated into the airborne particle collection device with a biosensor device that consists of a micro biochip, an optoelectronic detection architecture, and a wireless communication module (e.g., Bluetooth) transmitting the acquired data to a smartphone. The micro biochip inducing shear stress traps airborne particles into a polymer layer based on the pressure sensitive adhesive chemistry in the chamber, accordingly.

In this study, we have developed a micro-climate quality monitoring platform (Fig. 1). The platform enables us to demonstrate smartphone based integrated airborne microparticle collection and detection leading to automatic, real-time, and sensitive analysis. We first design and fabricate the collection device to collect airborne microparticle dispersed in the microclimate air. The optimal design and operating conditions of the collection device are determined using finite element analysis (FEA). Stabilized and consistent operation of the optimized collection device is demonstrated in a broad range of the airborne microparticles density in airflow. Furthermore, we construct the entire platform by integrating the collection device with an optoelectronic detection device that consists of a microfluidic particle trapping chamber and a complementary metal–oxide–semiconductor (CMOS) photodetector under a smartphone based communication. The platform effectively collects and detects airborne microparticle such as *Escherichia coli* (*E. coli*), *Bacillus subtilis*, *Micrococcus luteus,* and *Staphylococcus* of varying particle densities (from 10^3 to 10^8 CFL/mL) in less than one minute.

Experimental section

Materials and Chemical-/Biological-agents

Polystyrene (PS) particles (monosized standard spherical particle: 1µm in diameter; refractive index 1.59; density 1.06 g/cm^3; Duke Scientific Corporation, Palo Alto, CA, USA) was used to evaluate physical particle collection efficiency. The *Escherichia coli*, *Bacillus subtilis*, *Micrococcus luteus,* and *Staphylococcus* were purchased from Carolina biological supply (Burlington, NC, USA).

Finite element analysis

To predict the effect of the main design parameters impacting the performance of the airborne particle collection device and the biochip, we conducted FEA (COMSOL Multiphysics software) to obtain the particle trajectory, pressure distribution and velocity field in the airborne particle collection device and the biochip as a function of the geometric parameters (Table S2). The fluid drag force was estimated from the Khan and Richardson force.

Fabrication of airborne particle collection device

The airborne particle collection device consisted of three parts of air supply inlet, air sampling port, and channel body including outlet, designed on AutoCAD. Using a 3D printer (Prusa research, Prusa I3 MK3S) and a mechanical cutter, we obtained each part with polylactic acid (PLA). After printing the parts of the airborne particle collection device, we assembled and bonded together using acrylic cement (SCI-GRIP).

Fabrication of the biochip

The biochip consists of three parts; i) a top layer containing an inlet, an optical window, and an outlet, ii) a middle layer functioning as a micro chamber, and iii) a bottom layer playing roles of an adhesive layer and an optical window. The biochip was assembled the three pars cut from poly(methyl methacrylate) (PMMA) by a laser cutter (Versa Laser, ULS 4.60) by PSA (3M, 268L) films. Before the assembly step, we attached a PSA layer onto the channel bottom. To ensure the

integrity of the assembled device, after assembly, we pressed device using a hydraulic presses (Atlas Manual Press) under 7.5 tons for 30 min.

Integrated detector

For the integrated detection, firstly, we designed and fabricated a printed circuit board (PCB) (W×L×H = 64.7 mm × 31.2 mm ×1 mm) integrated with an Arduino Nano (WYPH, Arduino Nano). A commercial CMOS photodetector (ams, TSL2591) was connected to the Arduino Nano *via* I^2C communication protocol. The operation voltage of the photodetector and logic voltage of Arduino Nano are 3.3 V and 5 V, respectively. To compensate such discrepancy and make a stable I^2C communication, a level shifter circuit using two FET transistors (On Semiconductors, BSS138) was built. The logic levels of data (SDA) and clock (SCL) lines in the I^2C communication are biased as "High" at the idle condition. In order to wirelessly deliver sensor signal to outside iOS application, a Bluetooth BLE (DSD Tech, HM-10) was incorporated into the PCB. The operation voltage of each device was provided by a voltage regulator (Microchip Technology, MIC5225) which converts the applied voltage (9 V) to 3.3 V. Then, a microcontroller (MCU, ATMEGA328P) was combined with the as-fabricated PCB to control peripheral devices such as the CMOS photodetector, the voltage regulator, and the Bluetooth BLE (DSD Tech, HM-10). Finally, the integrated system with a light source (Luckylight, LL-S150W-W2-1C, I = 350 mcd) was enclosed by a package box printed out from a 3D printer (Prusa research, Prusa I3 MK3S). For the data communication and display, we employed Blynk [26] including an application software (https://blynk.io/) to construct IoT environment.

Bacterial particle preparation

All reactors were sterilized by autoclaving at 120 °C for 900 s. Bacterial particles were cultured to log phase at 37 °C with shaking of 200 rpm, and we harvested by centrifugation at 900g, washed twice with deionized (DI) water. We then suspended in DI water to ~10^6 CFU/mL and concentrated them by congregation at 900g for 10 min.

Airborne microparticle detection test

The aerosol generator, the biochip, and the airborne particle collection device were connected by PTFE tubing. By adjusting the concentration of microparticle suspension in the aerosol generator (BEIBERSI, BSW-2A, China), we controlled density of airborne microparticle in the airflow sample. By turning on the aerosol generator, uniform sized airborne particle distribution in the air was generated. When the air sample containing the defined concentration of airborne microparticle flew into the biochip, the airborne microparticles were captured into the biochip. The optical density change induced by the captured airborne microparticle particle was measured by the underneath CMOS.

Results and discussion

Integrated airborne particle collection device

We constructed the airborne particle collection device that does not need additional pumps since the pumping step for the collection of air samples hinders miniaturization and power effectiveness. In this study, the airborne particle collection device is intended to operate by means of the Venturi effect in a miniaturized platform to enable on-site sampling of airborne microparticle (Fig. 2). Since most indoor and microclimates involve heating, ventilation, and air conditioning (HVAC) system, by utilizing air flow generated by such HVAC systems in the indoor microclimate, the airborne microparticles are collected without additional power input to generate air flow. The airborne particle collection device consists of an air supply inlet, a vacuum gauge, a sampling port from the microclimate, and a discharge outlet (Fig. 2a). When air is supplied to the device through the inlet, a rapid pressure drop occurs around the inner constricted section of the device channel. The rapid pressure drop induces a suction of air containing airborne microparticles from the micro-climate environment. The airflow from the supply and sample sides are discharged through the outlet thereafter. The theoretical pressure drop due to Venturi effect at the constriction is estimated by $P_{air} - P_c = \rho_{air}/2\ (v_c^2 - v_{air}^2)$, where P_{air} is the pressure at the air supply inlet, P_c is the pressure of the constricted section, ρ_{air} is the density of air, v_c is the velocity of the constricted section, and v_{air} is the velocity of the air flow. Here, we chose P_{air} and the ratio between the diameter of the air supply inlet (D_{air}) and that of the constricted section (D_c), as design parameters. To set up the airborne particle collection device in a micro-climate, we targeted inside of the motor vehicle and defined the scale of the airborne particle collection device (Width × Height × Depth < 4 × 2 × 2 cm^3), we confirmed

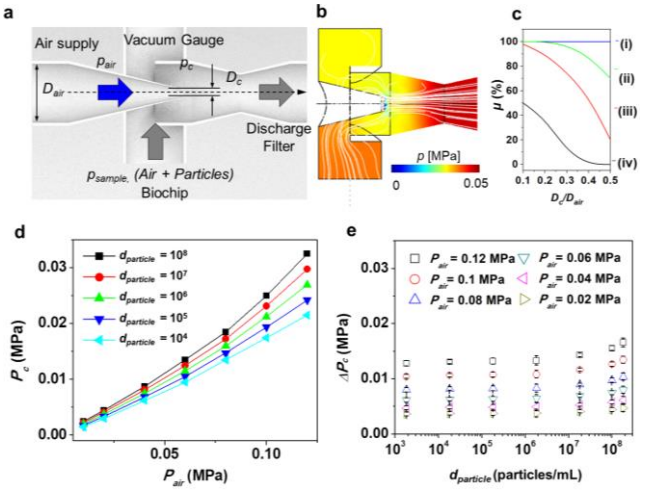

Fig. 2 integrative air-sample collection. a) Schematics of the airborne-pathogen collection based on Venturi effect. The airborne particle collection device consists of an air supply inlet, a vacuum gauge, a sampling port, and a discharge outlet. b) Pressure distribution in the airborne particle collection device at D_c/D_{air} = 0.2 and P_{air} = 0.1 MPa. c) D_c/D_{air} effect on η_C at P_{air} = i) 10^{-1}, ii) 10^{-2}, iii) 10^{-3}, and iv) 10^{-4} MPa. d) Measured P_c and e) ΔP_c as a function of P_{air} and $d_{particle}$, respectively.

the concept of the airborne particle collection device by using FEA (see "Experimental" section and Fig. S1) (Fig. 2b). In this analysis, we calculated the particle trajectories by solving the ballistic equation of motion for each microparticle. It was assumed that a spherical particle with a mass (m) and a radius (r_p) in the air flow with a density (ρ) and a dynamic viscosity (η) was subjected to gravitational forces, the hydrodynamic Stokes' drag, and the related buoyancy. The fluid drag force was estimated from the Khan and Richardson force, which is given for a wide range of Reynolds numbers as:

$$F = \pi r_p^2 \rho(\bar{u} - \bar{u}_p)^2(1.84Re_p^{-0.31} + 0.293Re_p^{0.06})^{3.45}, \quad (1)$$

$$Re_p = (|\bar{u} - \bar{u}_p|2r_p\rho)/\eta$$

where, u represents the fluid velocity, and u_p represents the particle velocity. To predict the fluid drag force based on Eq. (1), we solved the incompressible Navier–Stokes equation and the continuity equation to obtain the air velocity field, u_p and P in the airborne particle collection device. Considering the asymmetric shape of the device, the computational system was constructed using a 3D model (Fig. S1). The pressure distribution and particle tracing at D_c/D_{air} = 0.2 (D_{air} = 1 cm), P_{air} = 10^{-2} MPa shows that P_c generation results in the induction of particles (r_p = 1 μm) flowing from the micro-climate side. We also estimated the particle collection efficiency ($\eta_C = n_c/n_s \times$ 100%, where n_s is the number of particles injected into the sampling area and n_c is the number of particles at the constriction area), as a function of D_c/D_{air} and P_{air} (Fig. 2c). The estimated η_C rapidly increases from 0 to 100% as either P_{air} increases from 10^{-4} to 10^{-1} at D_c/D_{air} is 0.1 or D_c/D_{air} decreases from 0.5 to 0.1 when P_{air} is above 10^{-2} MPa. These FEA results indicate that Venturi effect in the airborne particle collection device design allows high negative pressure to induce particle collection in airflow for the miniaturized platform.

In order to confirm the airborne particle collection device operation at the different densities of airborne microparticles in the microclimate, we first measured the negative pressure at the constricted zone by installing the vacuum gauge in the airborne particle collection device when air is injected into the air supply inlet (Fig. S2). As a representative microparticle, we tested 1 μm-dia. polystyrene (PS) beads along with varying densities ($d_{particle}$) (see "Experimental" section). Fig. 2d plots the measured P_c as a function of P_{air} from 0 to 0.12 MPa at varying $d_{particle}$ from 10^4 to 10^8 particles/mL. P_c increased with P_{air}. In addition, higher $d_{particle}$ led to higher P_c, however variation of P_c ($\Delta P_c = P_{c\_air} - P_{c\ particle}$, where P_{c_air} and $P_{c\ particle}$ are the pressure of constricted section of airflow without and with particles, respectively) as a function of $d_{particle}$ between10^3 and 10^8 particles/mL does not show significant changes (Fig. 2e). For instance, even at P_{air} = 0.08 MPa, ΔP_c varied from 0.007 to 0.01 MPa with $d_{particle}$ ranging from 10^3 to 10^8 particles/mL. In such a wide range of $d_{particle}$, the airborne particle collection device enables the collection of airborne microparticles without any clogging and dramatic change of pressure issues.

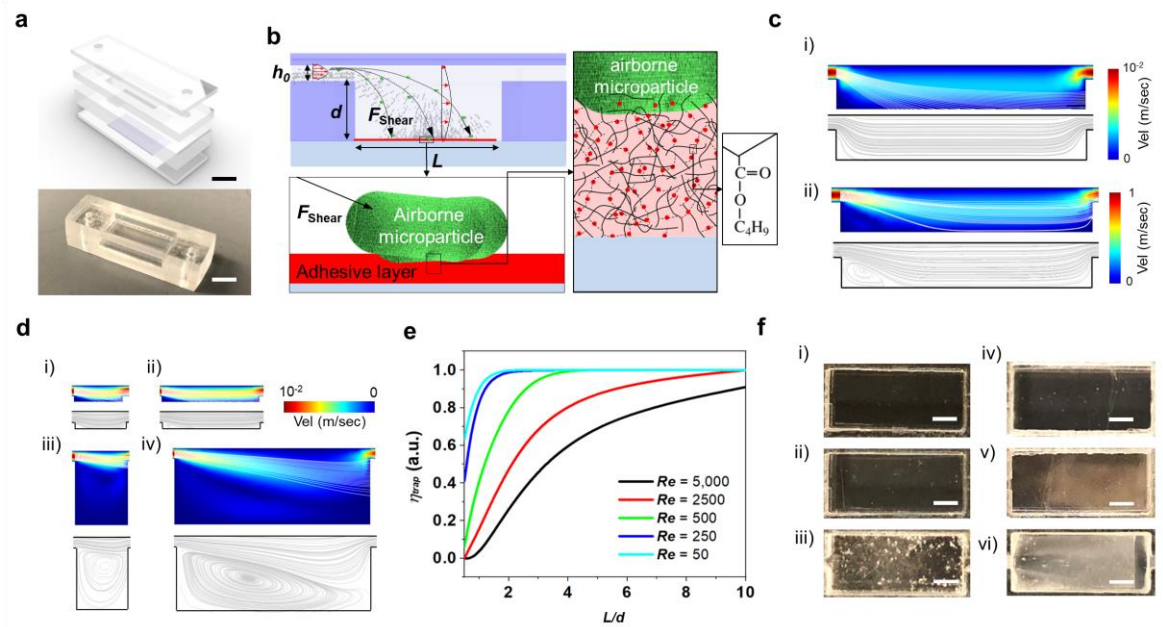

Fig. 3 Airborne microparticle detection biochip. a) Design and photo image of the detection biochip (scale bar = 2 mm). b) Schematic illustration of the airborne microparticle trapping in the biochip. i) In the chamber expanded suddenly, the inertia force driven drag force leads to move the airborne microparticles forward to the bottom of the chamber. ii) a pressure-sensitive polymer (butyl acetate) is placed on the bottom of the chamber. iii) The drag force of the airborne microparticle on the pressure-sensitive adhesive results in polymerization of the adhesive layer and strong bonding. iv) The strong binding between the adhesive layer and the airborne microparticles allows avoiding the detachment of the trapped the airborne microparticles, although local vortex or swirling of the airflow can occur. c) Velocity distribution (color profile), particle trajectory (white curves), and streamline (grey curves) at Re = 5 and 500. d) Velocity distribution (color profile), particle trajectory (white curves), and streamline (grey curves) at various geometry of L/d = 10 and 20 at h_0 (= 0.5 mm)/d = 1 and L/d = 0.5 and 10 at h_0 (= 0.5 mm)/d =5. e) Particle trapping efficiency estimated without consideration of the adhesion layer on the bottom of the chamber as a function of L/d from 1 to 10 at h0 = 0.5 mm and variation of *Re* between 50 and 5,000. f) Photo images of trapped microparticles in the biochip (h_0 = 0.5 mm, d = 4 mm, and L = 12 mm) at $d_{particle}$ = 10^6 particles and Re = i) 0, ii) 5, and iii) 50 without adhesive layer and Re = iv) 0, v) 5, and vi) 50 with an adhesive layer (Scale bar = 2 mm).

Biochip to trap airborne microparticle

With the airborne microparticle collection performance of airborne particle collection device, to demonstrate the real-time monitoring of the particle density, we constructed an integrated airborne microparticle detection system (Fig. 3). First, we designed a microfluidic biochip consisting of the inlet, trapping chamber and outlet to capture airborne microparticles in the air sample using a concept of the inertia flow (Fig. 3a and see Experimental section). The inertia flow concept enables the operation of the detection system with minimal pressure drop, unlike conventional systems based on the filtering. The minimal pressure drop, which does not need pumping and mechanical parts to support high pressure operation, allows a miniaturized detection system. Although this concept of inertial flow based microfluidic device have been studied and reported [27, 28], these studies have been focused on aqueous phases and larger microparticles (r_p > 5 μm). Since air flow revealing low viscosity leads to eddy flows or vortexes in the micro device, to trap airborne microparticles in the microchip, an advanced design is necessary.

In the microfluidic biochip, the collected air sample enters a narrow inlet channel and then flows into a larger chamber space. In the larger height chamber, the velocity of the particles becomes slower due to a larger gravitational force and lower kinetic energy. This leads to the settling of the particles at the bottom of the microfluidic chamber. The pressure-sensitive polymer (butyl acetate) is placed on the bottom of the chamber. The shear stress between the airborne microparticle and the pressure-sensitive adhesive layer results in polymerization of the adhesive layer and strong bonding. This strong binding allows avoiding the detachment of the trapped airborne microparticles, although local vortex or swirling of the airflow (Fig. 3b).

We estimated the velocity profiles, particle trajectories, and streamlines for different and the particle-capture efficiency in the designed biochip for different inlet velocities and chamber geometries using FEA (Fig. 3c, d and Fig. S3). Lower inlet velocity (*Re* = 50) results in a symmetric velocity profile and settling the particles on the bottom of the chamber, while a higher one (*Re* = 500) shows an asymmetric velocity profile with fewer numbers of settling particles. In addition, we investigated the geometric effect of channel height (h_0) = 1 mm, chamber depth (d) = 4 mm, and chamber length (L) on the particle trapping into the chamber. Larger eddy occurs with d/h_0, while L/d does not show clear trends in the eddy size. Meanwhile, longer L/d leads to a larger number of particle trapping in the micro chamber. Based on the analysis results, particle capturing efficiency (η_{trap}) is close to 100% when *Re* at the inlet is kept below 250 at d = 4 mm, and chamber length L = 12 mm when h_0 is 1 mm (Fig 3e). Furthermore, the high ratio of the channel length to depth (L/d > 3) leads to η_{trap} = ~ 100 %. Once the flowing particles touch the bottom- / side- wall of the biochip chamber, they are affected by shear stress [29]. This means that they are captured effectively. Furthermore, to ensure the remaining attachment of the captured airborne microparticles, we employed a pressure sensitive adhesion layer on the bottom surface of the microfluidic chamber (Fig 3f). We observed minimal aggregation in the biochip with the adhesive layer, meanwhile, the particle aggregation existed when there was no adhesion layer (control). The adhesive layer in the biochip led to uniform distribution and less particle aggregation. The total number of airborne microparticles retained in the chamber can be determined by the loading time and the concentration of microparticle in suspension. This means that the biochip can play a reliable role as an indicator of the number of the microparticle in the airflow.

Integrated airborne microparticle detection platform

Having the biochip, we constructed the detection device consisted of the biochip, a light-emitting diode (LED), as a light source, a CMOS photodetector, a microcontroller unit (MCU), and a Bluetooth module with a PCB (Fig. 4, Fig. S4 and see "Experimental" section). The microparticle trapping in the biochip leading to changes in the optical transmission is detected by the underneath CMOS photodetector under light illumination from the top LED (Fig. 4a). The change of optical transmission results in the photocurrent (I) change through the integrated CMOS photodetector (Fig. S5). The measured I represents the density of the trapped particles from the airflow collected by the airborne particle collection device. In detail, the operation involves i) supplying air into the airborne particle collection device to generate negative pressure and induce the collection of air sample containing airborne microparticles from the microclimate, ii) flowing the collected air sample into the biochip, iii) capturing microparticles in the

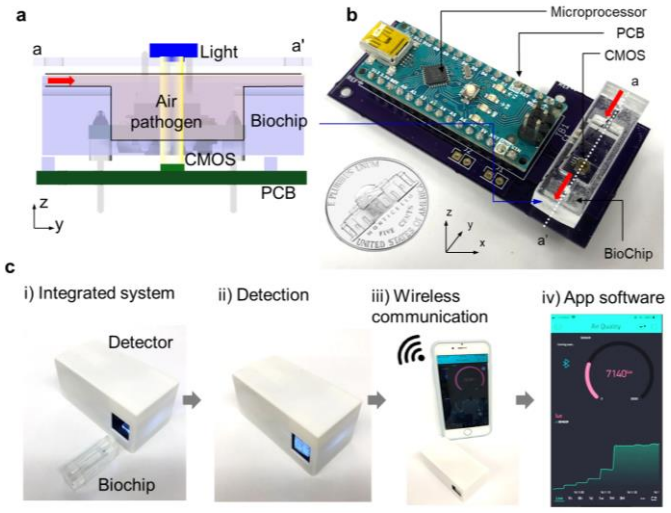

Fig 4. integrated microparticle detection system. a) Photograph image of the integrated detection system. The microparticle contained air sample is loaded into the biochip inlet via negative pressure induced by the airborne particle collection device connected at the outlet of the biochip. b) Alignment between an upper light source, a biochip trapping airborne microparticles, and a underneath CMOS detector. c) Operation; i) Enclosed detection system and biochip, ii) Detection loaded biochip, iii) wireless communication between the integrated detection system and a smartphone, and iv) an application-software (Bylnk Internet on thing (IoT) Platform) for real-time data acquisition and display.

air sample into the biochip, iv) measuring a change of optical transmission under light illumination, v) transmitting the measured optical-signal change to a smartphone, and vi) displaying the measured results through the installed application software (Fig. 4c and Fig. S6). After completion of the detection and the data acquisition, the used biochip was replaced with a new one for the next measurement. This permits a recycled use of the same CMOS photodetectors and the LED. The pixel size of the CMOS detector (3 mm x 1.5 mm) underneath the micro chamber is large enough to cover more than 50% of the particle detection area (i.e., the bottom surface) of the micro chamber. This allows the detector to measure photo signals spatially averaged over a majority (~80%) of trapped microparticles according to the prediction in Fig. 3c. The detection of the spatially averaged signal is expected to limit the effect of the particle distribution on our measurement.

Airborne microparticle collection and detection

We performed airborne microparticle collection and detection tests (Fig. 5). For these tests, airborne pathogen microparticles of *E. coli*, *Bacillus subtilis*, *Micrococcus luteus*, and *Staphylococcus* were used as target airborne microparticles. These airborne pathogens have been clinically known as the critical sources in a variety of infections[4, 5] and severe respiratory diseases [6, 7]. We validated the trapping of the airborne microparticles in the biochip chamber by obtaining a scanning electron microscope (SEM) image (Fig. 5a (i)). At P_{air} = 0.05 MPa, after flowing the airflow sample with 10^5 CFU/mL of *E. coli* density ($d_{E.\ coli}$) for 60 sec, the obtained SEM image indicates that the experimental setup enabled to collect and trap the airborne microparticle. The photographic images of the surface of the biochips show that light extinction is varied as a function of $d_{E.\ coli}$ from 0 to 10^8 CFU/mL (Fig. 5a (ii)). Then, we performed the airborne microparticle detection using the integrated system of the airborne particle collection device and the biochip as a function of $d_{E.Coli}$ (Fig. 5b). Depending on the airborne microparticle density, the change of optical transmission in the biochip leads to different photocurrent signals (I) from the CMOS photodetector. The variation of the measured photocurrent ($\Delta I/I_0$) is a function of $d_{E.coli}$. After loading *E. coli* samples into the aerogel generator, the air sample flow was generated by the airborne particle collection device, and we subsequently measured the $\Delta I/I_0$ as a function of $d_{E.\ coli}$ from 10^3 to 10^8 CFU/mL (see Experimental section). The $\Delta I/I_0$ rapidly increases for the first 60 seconds and gradually reaches a plateau regardless of $d_{E.\ coli}$. For instance, when $d_{E.\ coli}$ is 10^5 CFU/mL, $\Delta I/I_0$ is 0.025 at t = 60 seconds, and slightly increases to 0.05 for next 300 seconds. Quantification of *E. coli* density in the air samples was enabled in such a short detection time. Based on the dependency of the $\Delta I/I_0$ on the particle density, we constructed a calibration curve of $\Delta I/I_0$ as a function of particle density in the air sample (Fig. 5c-f). While the airborne particle collection device operates, the biochip enabled the detection of the airborne pathogens; *Bacillus subtilis*, *Micrococcus luteus*, and *Staphylococcus* from 10^3 to 10^8 CFU/mL. The estimated limit of detection (LOD) of the integrated system of the airborne particle collection device and the biochip for *E.coli* in an airflow is as low as 411 CFU/mL according to $3\sigma/k_{slope}$ (σ is the standard deviation of the background signal measured from a blank control. k_{slope} is the

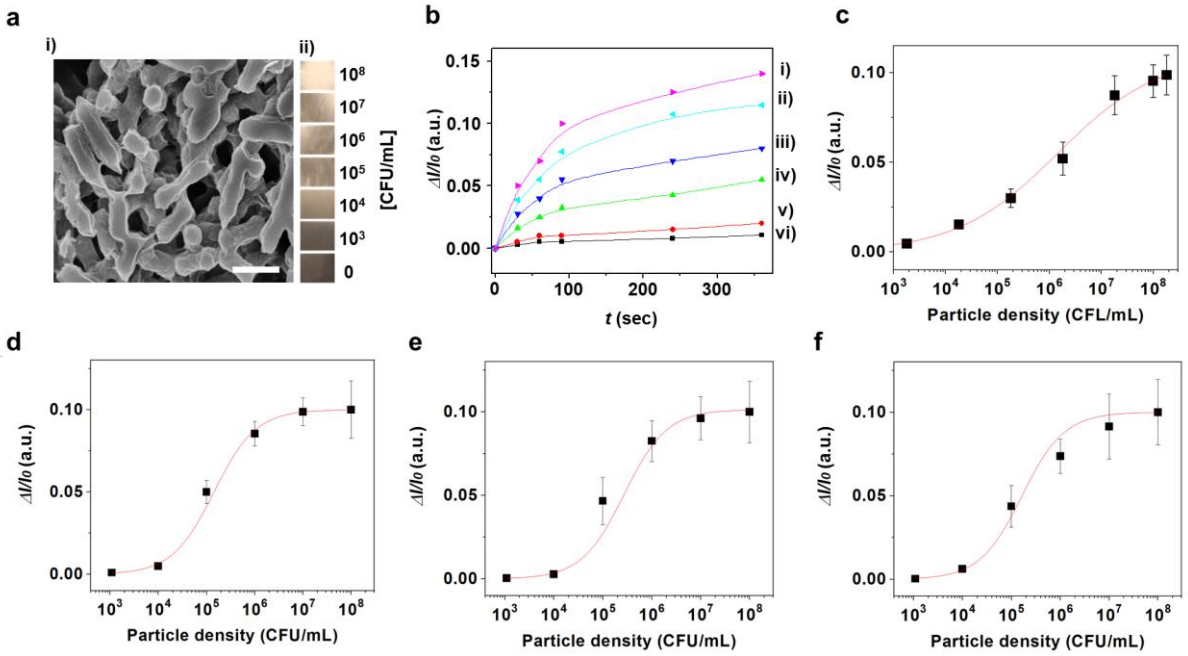

Fig. 5. Airborne pathogen particle detection tests. a) i) SEM image of trapped *E. coli* particles in the biochip (h_0 = 1 mm, d = 4 mm, and L = 12 mm) at V_{inlet} = 0.01 m/sec (scale bar = 1 μm) and ii) photograph images of the surface of the same dimension of biochips as a function of $d_{E.\ coli}$ from 0 to 10^8 CFU/mL. b) Dynamic $\Delta I/I_0$ as a function of $d_{E.coli}$ at i) 10^3, ii) 10^4, iii) 10^5, iv) 10^6, v) 10^7, and vi) 10^8 CFU/mL. c) Calibration curve of *E. coli*, d) *Bacillus subtilis*, e) *Micrococcus luteus*, and f) *Staphylococcus* detection in the integrated detection system.

regression slope of the calibration curve). Considering their different shapes, sizes, surface charges, and membrane structures, we chose these airborne pathogens as reprehensive test models. We listed their structural properties and clinically related diseases in Table S3. Fig. S7 shows the LODs of the integrated system for the airborne microparticles according to the constructed calibration curves. The estimated LODs are ~620, ~280, and ~400 CFU/mL for *Bacillus subtilis*, *Micrococcus luteus*, and *Staphylococcus,* respectively. These results indicated that the integrated system consistently performed effective collection and detection performance, regardless of the shape, size, and surface charge of the microparticles. In addition, we designed the sample collector so that its geometry allows particles within a narrow mass range, such as bacteria particles (density = ~ 1.1166 ± 0.0007 g/ml), to be selectively collected. Specifically, the mass-specific particle collection was arranged by carefully choosing the ratio between the contraction and air supply sizes. To make the integrated sample collection and detection system available for broader use, our investigation is underway to understand the effects of the geometry and multistage arrangement of the collector on particle collection.

Conclusions

We successfully demonstrated an integrated on-site system for the rapid and sensitive airborne microparticle detection for indoor air-quality monitoring. The airborne particle collection device inspired by Venturi effect enabled an effective and miniaturized microparticle collection. The optimized airborne particle collection device resulted in consistent operation by showing a minimal pressure change when subjected to a wide range of micro-particles with varying densities in the airflow. We constructed an integrated airborne microparticle detection system enabling wireless communication module transmitting the acquired data. Subsequently, the airborne particle collection device and the biochip effectively collected and detected airborne microparticles such as *E. coli*, *Bacillus subtilis*, *Micrococcus luteus*, and *Staphylococcus* with high sensitivity under particle densities from 10^3 to 10^8 CFU/mL in less than one minute. The practical implementation of the demonstrated system further requires specificity in its particle detection. We are currently working to introduce high detection specificity to our system by incorporating a biosensing feature that distinguishes the types of the collected airborne microparticles into the biochip based on either mass/size particle sorting, specific particle-receptor binding, or selective particle-labelling mechanism.

Conflicts of interest

There are no conflicts to declare.

Acknowledgements

This work was supported by Ford Motor Company, academic research fund, and the National Science Foundation (CBET 2030551). Also this work was funded by grant from Mcubed U064088.

References

1. Gubbi J, Buyya R, Marusic S, Palaniswami M. Future Generation Computer Systems 2013;29:1645-60.
2. Khan R, Khan SU, Zaheer R, Khan S. 2012 10th International Conference on Frontiers of Information Technology 2012. p. 257-60.
3. Mehmood Y, Ahmad F, Yaqoob I, Adnane A, Imran M, Guizani S. IEEE Communications Magazine 2017;55:16-24.
4. Jo WK, Lee JH. Archives of environmental & occupational health 2008;63:101-7.
5. Stephenson RE, Gutierrez D, Peters C, Nichols M, Boles BR. Biofouling 2014;30:337-46.
6. Amabile N, Heiss C, Real WM, Minasi P, McGlothlin D, Rame EJ, et al. American Journal of Respiratory and Critical Care Medicine 2008;177:1268-75.
7. McVey M, Tabuchi A, Kuebler WM. American Journal of Physiology-Lung Cellular and Molecular Physiology 2012;303:L364-L81.
8. Bouley G, Dubreuil A, Despaux N, Boudene C. Scandinavian Journal of Work, Environment & Health 1977;3:116-21.
9. D'Amato G. Allergy 2001;56:1109-11.
10. Kumar P, Lopez M, Fan W, Cambre K, Elston RC. Annals of allergy 1990;64:174-7.
11. Ho Y-P, Reddy PM. Mass Spectrometry Reviews 2011;30:1203-24.
12. Pan Y-L, Boutou V, Bottiger JR, Zhang SS, Wolf J-P, Chang RK. Aerosol Science and Technology 2004;38:598-602.
13. Pybus OG, Rambaut A. Evolutionary analysis of the dynamics of viral infectious disease. Nature Reviews Genetics 2009;10:540-50.
14. Varshney M, Li Y, Srinivasan B, Tung S. Sensors and Actuators B: Chemical 2007;128:99-107.
15. Pasanen AL. Indoor air 2001;11:87-98.
16. Glasgow HB, Jr., Journal of toxicology and environmental health 1995;46:501-22.
17. Hogan CJ, Jr., Kettleson EM, Lee MH, Ramaswami B, Angenent LT, Biswas P. Journal of applied microbiology 2005;99:1422-34.
18. Jia Y, Fraser M. Environmental Science & Technology 2011;45:930-6.
19. Heidelberg JF, Eisen JA, Nelson WC, Clayton RA, Gwinn ML, Dodson RJ, et al. Nature 2000;406:477-83.
20. Lee KS, Bartlett KH, Brauer M, Stephens GM, Black WA, Teschke K. Indoor air 2004;14:360-6.
21. Choi J, Hong SC, Kim W, Jung JH. ACS Sensors 2017;2:513-21.
22. Choi J, Kang M, Jung JH. Scientific Reports 2015;5:15983.
23. Fronczek CF, Yoon JY. Journal of laboratory automation 2015;20:390-410.
24. Fung AO, Mykhaylova N. Journal of laboratory automation 2014;19:225-47.
25. Liu Q, Zhang Y, Jing W, Liu S, Zhang D, Sui G. The Analyst 2016;141:1637-40.

26. Blynk hwbi, " Blynk, 2017. [Online]. Available:, https://www.blynk.io/.
27. Dimov IK, Kijanka G, Park Y, Ducrée J, Kang T, Lee LP. Lab on a Chip 2011;11:2701-10.
28. Zhang X-B, Wu Z-Q, Wang K, Zhu J, Xu J-J, Xia X-H, et al. Analytical Chemistry 2012;84:3780-6.
29. Manbachi A, Shrivastava S, Cioffi M, Chung BG, Moretti M, Demirci U, et al. Lab on a chip 2008;8:747-54.

